Journal of Superconductivity and Novel Magnetism (2024) 37:1965–1975
https://doi.org/10.1007/s10948-024-06796-5

RESEARCH

Manometric Determination of the Oxygen Diffusion Coefficients in $YBa_2Cu_{3-y}Fe_yO_{6+x}$

J. Kargin[1] · H. E. Sanchez Cornejo[2] · K. Zhangozin[3] · T. Zhanabergenov[3] · Zh. Kassymkhanov[1] · Jiwon Seo[4] · S. N. Holmes[5] · C. H. W. Barnes[6] · J. Albino Aguiar[7] · L. De Los Santos Valladares[6,7]

Received: 5 March 2024 / Accepted: 27 June 2024 / Published online: 13 July 2024

Abstract

Thermodynamic parameters, such as the activation energy (E_a) and the diffusion coefficient (D_0), of weakly bounded oxygen in Fe-doped $YBa_2Cu_3O_{6+x}$ ($YBa_2Cu_{3-y}Fe_yO_{6+x}$) system were obtained utilizing the Manometric technique. It is found that under isothermal conditions, oxygen desorption in $YBa_2Cu_3O_{6+x}$ (YBCO) occurs following an exponential decay trend and in two distinct stages. During the first stage, the majority of absorbed oxygen is released, while the second stage exhibits a delayed degassing kinetics. E_a and D_0 were determined for both, pressed and powdered, samples of the YBCO and $YBa_2Cu_{3-y}Fe_yO_{6+x}$ systems, from experimental kinetic curves, depicting gas release $P(t)$ under isothermal vacuum degassing conditions. It is demonstrated that doping with Fe prevents oxygen exchange in YBCO, as evidenced by the reduction in the quantity of released oxygen with increasing iron index (y). The experimental results validate the efficacy of the Manometric method for analyzing and determining the thermodynamic and kinetic properties of the YBCO superconductor.

Keywords YBCO · Manometry of superconductors · Oxygen diffusion coefficients · Superconductors

1 Introduction

The $YBa_2Cu_3O_{6+x}$ (YBCO) system, with $0 < x < 1$, exhibits a plethora of structures and superstructures, primarily induced by doping with transition metals and variation in oxygen content [1–4]. In fact, YBCO stands out as a unique compound in which a small change in oxygen concentration in the basal plane immediately leads to a big change in structure and magnetic and electrical properties [5–12]. Consequently, studying the kinetic of oxygen in high critical temperature superconductor (HTSC) type 123 remains a pressing concern, captivating the attention of numerous investigators [13]. Over the years, various methods have been employed to study the diffusion of oxygen in HTSC phases [12–21], encompassing dynamic [14] and isothermal [15] thermogravimetry, electrochemical potentiometry [16], distribution of the $^{18}O/^{17}O$ isotopic label [17–19], determination of internal friction coefficients [18], in situ measurements of electrical resistance [20], direct observations of twinning front propagation in single crystals [21, 22], isotope exchange method with the gas phase [23, 24], and computer modeling [25].

Despite the significant divergence in results reported by different researchers, caused by methodological diversity

✉ J. Kargin
kjb_orken@mail.ru

✉ L. De Los Santos Valladares
ld301@cam.ac.uk

1 L.N. Gumilyov, Eurasian National University, NPJSC, Astana, Kazakhstan

2 Laboratorio de Ceramicos y Nanomateriales, Facultad de Ciencias Físicas, Universidad Nacional Mayor de San Marcos, Ap. Postal 14-0149, Lima, Peru

3 TSK-Vostok, Astana, Kazakhstan

4 College of Science and Technology Convergence, Yonsei University, 1 Yonseidae-gil, Wonju, Gangwon-do 26493, South Korea

5 Department of Electronic and Electrical Engineering, University College London, Torrington Place, London WC1E 7JE, UK

6 Cavendish Laboratory, Department of Physics, University of Cambridge, J.J. Thomson Ave, Cambridge CB3 0HE, UK

7 Programa de Pós-Graduação em Ciências de Materiais, Centro de Ciências Exatas e da Natureza, Universidade Federal de Pernambuco, Recife, PE 50670-901, Brazil

and influencing factors on oxygen diffusion, certain patterns have emerged; the coefficients of self-diffusion and chemical diffusion are interconnected by a simple relationship: $D_{chem} = \Phi D_{self}$, where Φ is the thermodynamic factor. It is noted that the chemical diffusion coefficient (D_{chem}) surpasses the self-diffusion coefficient (D_{self}) by four to five orders of magnitude. For YBCO polycrystalline samples, D_{chem} typically ranges from 10^{-5} to10^{-11} cm^2/s, while D_{self} falls between 10^{-9} and 10^{-13} cm^2/s. In rare earth-123 systems, the activation energy for self-diffusion decreases with increasing ionic radius of the rare earth element. The second-order phase transitions during oxygen sublattice ordering, or disordering, are expected to result in abrupt changes in the diffusion coefficients. In the orthorhombic phase, oxygen diffusion occurs faster than in the tetragonal phase, despite the latter containing more available oxygen vacancies.

This study aims to experimentally determine the diffusion coefficients of oxygen in $YBa_2Cu_3O_{6+x}$ samples using the method of isothermal vacuum degassing and to explore the impact of iron doping on the kinetic parameters of oxygen in $YBa_2Cu_{3-y}Fe_yO_{6+x}$.

2 Theoretical Considerations

2.1 Determination of the Kinetic Parameters

The determination of the kinetic parameters and the quantity of oxygen absorbed by the samples during vacuum degassing was conducted by considering continuous pumping conditions. The dynamics of the pressure variation of the released gas in the system can be expressed by the following equations:

$$VdP = Jdt - SPdt \tag{1}$$

or

$$\frac{dP}{dt} + AP = \frac{J}{V} \tag{2}$$

where $J(t)$ is the rate of gas release from the sample; V is the volume of the measuring cell together with the recording sensor (Pirani pressure gauge); S is the effective gas pumping speed; $A = S/V$ is a "pumping constant" which can be determined by continuously evacuating a portion of the oxygen previously introduced into the system at a pre-defined pressure value P_0, and in the absence of the sample. In this scenario, the pressure in the system during pumping changes according to an exponential law, expressed as:

$$P = P_0 e^{-At} \tag{3}$$

Furthermore, the constant A can be ascertained from the slope of the straight line plotted in the "lnP-t" coordinates.

A characteristic representation of the gas release curve from the sample in P vs. t coordinates is depicted in Fig. S1 in the supporting material. In the figure, $t = t_0$ marks the moment of time counted from the starting of sample heating ($t = 0$), designated as the starting point for time counting when analyzing the kinetic curve for the isothermal degassing interval. The initial segment of the releasing-gas-curve $P(t)$ to the maximum corresponds to heating the sample to a specific temperature, while the descending portion of the curve corresponds to the isothermal degassing.

As a general rule, the rate of gas released from the sample (J) undergoes a time-dependent change following an exponential law given by

$$J = J_0 e^{-kt} \tag{4}$$

Here, J_0 is a constant, and k is the degassing coefficient characterizing the rate of gas released from the sample and dependent on the experiment's temperature. The exponential time law in Eq. (4) is characteristic and can manifest various mechanisms of the limiting stage of the gas evolution process. Specifically, this occurs in scenarios such as limited diffusion inside materials (regular mode at sufficiently long times), first-order surface reaction, and desorption of molecules adsorbed without dissociation.

From Eqs. (2) and (4), and considering the times t_0 and t, it follows

$$ln\left\{\frac{\frac{dP/dt}{A} + P}{\frac{dP_0/dt}{A} + P_0}\right\} = -k\Delta t \tag{5}$$

where $\Delta t = t - t_0$. The kinetic parameter k, as inferred from Eq. (4), can be obtained from the slope of a straight line constructed in the coordinates:

$$ln\left\{\frac{\frac{dP/dt}{A} + P}{\frac{dP_0/dt}{A} + P_0}\right\} \text{vs } \Delta t$$

Assuming that the temperature dependence of k follows the Arrhenius equation, by obtaining a series of k values related to different degassing temperatures and plotting the dependence of $\ln(k)$ on $1/T$ (where T is the temperature, in K), the activation energy of the process (E_a) can be determined.

The activation energy of the releasing-gas process can be determined either graphically or by the least squares method, from the slope of the curve representing the dependence of $\ln(k)$ vs $1/T$, i.e.,

$$E_a = -\left(\frac{\Delta lnk}{1/T}\right)R, \text{where } R \text{ is the gas constant.}$$

By integrating Eq. (1) over the degassing period from $t=0$ to $t=\infty$, in which the oxygen pressure in the system changes from the background value (P_{ϕ}), passing through the maximum and returning to the background value P_{ϕ}, the following expression is obtained:

$$V\int_{P_{\Phi}}^{P_{\Phi}} dP = 0 = \int_0^{\infty} Jdt = S\int_0^{\infty} Pdt, \tag{6}$$

Since the integral $\int_0^{\infty} Jdt = S\int_0^{\infty} Pdt$ is the value Q (expressed in Pa×m^3) and proportional to the total number of particles released from the sample during the entire degassing time, and the integral $\int_0^{\infty} Pdt$ represents the area under the $P(t)$ curve (area expressed in Pa×s), then Eq. (6) establishes the proportionality between Q and the area under the curve $P(t)$, i.e.,

$$Q = S\int_0^{\infty} Pdt \tag{7}$$

To convert the value Q into moles (Q'), both sides of Eq. (7) should be divided by RT, where T is the temperature near the measuring sensor and R is the gas constant. Then,

$$Q\prime = \frac{S}{RT}\int_0^{\infty} Pdt = \frac{\alpha}{T}\int_0^{\infty} Pdt \tag{8}$$

where $\alpha = S/R$ (mol×K/Pa×s) is a constant determined experimentally, and it is also similar to the constant A described above.

Considering that the gas pressure p' in the selected volume V' is known, the number of moles of the substance Q' can be expressed as

$$Q' = \frac{p'V'}{RT} \tag{9}$$

Therefore,

$$\alpha = \frac{Q'T}{\int_0^{\infty} Pdt} = \frac{P'V'}{R\int_0^{\infty} Pdt} \tag{10}$$

where T is the temperature near the installation.

To describe the diffusion of oxygen inside the $YBa_2Cu_3O_{6+x}$ pellets, a model was developed for the diffusion in a semi-limited sample with initial concentration C_0 through the surface ($y=0$) into a medium that does not contain a diffusing substance. Then, maintaining a zero concentration $C(0,t)=0$ [26]:

$$C(y,t) = C_0 erf\frac{y}{2\sqrt{Dt}}, \tag{11}$$

where *erf* stands for "error function." The quantity of substance q passing through a unit surface during time t is determined as the integral of the flow over time, i.e.,

$$q = \int_0^t jdt = -D\int_0^t \left\{\frac{dC}{dy}\right\}_{y=0} dt = \left\{\frac{2}{\sqrt{\pi}}\right\} C_0\sqrt{Dt} \tag{12}$$

When transitioning from the total amount of substance q released from the sample to a value in the non-stoichiometry oxygen state ($\Delta x = x - x_0$), Eq. (12) takes the form:

$$\Delta x = x_0\left\{\frac{2S}{V\sqrt{\pi}}\right\}\sqrt{Dt} \tag{13}$$

where x_0 is the initial value of the parameter x, determined from the phase diagram with known values of P_{O_2} and T; S and V are the surface area and volume of the sample, respectively, and D is the diffusion coefficient. Squaring Eq. (13), the values of the oxygen diffusion coefficient can be determined from the slope of the curve $(\Delta x)^2 = f(t)$.

2.2 Vacuum Degassing of $YBa_2Cu_3O_{6+x}$

To account the geometric influence, the pressed YBCO sample underwent pulverization in an agate mortar, after which the kinetic parameters were estimated. The powders were placed in an Alundum crucible and located inside a quartz holder. Under oxygen flow at the required partial pressure, the $YBa_2Cu_3O_{6+x}$ powders were then subjected to heating to the desired temperature and maintained until the saturation with oxygen was attained. Subsequently, the sample was moved to the cold zone of the furnace, and the oxygen in the entire system was evacuated to a background pressure (10^{-6} mmHg = 133.3 μPa) while simultaneously annealing the system at 800 °C. Upon reaching the background pressure, the designated degassing temperature was set in the reactor, which remained constant throughout the whole degassing process, and under continuous system pumping.

The curve illustrating the changes in oxygen pressure, denoted as $P(t)$, exhibited the characteristic shape depicted in Fig. S1. The descending segment in the releasing-gas-curve corresponds to conditions of isothermal degassing. The analysis of the experimental $P(t)$ curves revealed that under isothermal conditions, for at least 90% of releasing of the absorbed oxygen, the rate for releasing oxygen from the $YBa_2Cu_3O_{6+x}$ sample can be described by Eq. (4), where J_0 represents the initial rate of oxygen release at $t=0$, and k is the desorption constant.

In this scenario, the concentration distribution $C(r,t)$ in a sample with a shape of a solid sphere with radius b, is determined by solving the following form [26]:

$$\frac{C - C_0}{C_1 - C_0} = 1 + \frac{2b}{\pi r}\sum_{n=1}^{\infty}\frac{(-1)^n}{n} sin\frac{n\pi r}{b} exp\left(-\frac{Dt\pi^2 n^2}{b^2}\right) \tag{14}$$

where C_0 is the initial oxygen concentration, C_1 is the final equilibrium oxygen concentration, t is the duration time of isothermal annealing, and $D = Do \times exp(-E/RT)$ is the diffusion coefficient of oxygen (in cm^2/s).

In the present work $C(r,0) = C_0$ and $C(b, t) = C_1 = 0$, then the oxygen flow j per unit area looks like as follows:

$$j = -D\left.\frac{dC}{dr}\right|_{r=b} = -\frac{2C_0}{b}\sum_{m=0}^{\infty} exp\left(-\frac{(2m+1)^2\pi^2}{b^2}Dt\right)\cos(2m+1)\pi \tag{15}$$

where r is the radius of a spherical particle (in cm), and m is whole numbers 0,1,2,3…∞.

After a long time (regular approximation), the main contribution to this sum comes from the first term of the expansion ($m = 0$), and the releasing-gas-law (Eq. 15) coincides with an exponential law (Eq. 4), i.e.,

$$q = -DS\int_0^t \left(\frac{dC}{dr}\right)_{r=b} dt = -\frac{2C_0 bS}{\pi^2} exp\left(-\frac{\pi^2 Dt}{b^2}\right) \tag{16}$$

Expressing Eq. (16) through the oxygen parameter x, the following relation is obtained:

$$\Delta x = x_0\left\{\frac{2bS}{V\pi^2}\right\} exp\left(-\frac{\pi^2 Dt}{b^2}\right), \tag{17}$$

since $S/V = 3/b$, then the equation becomes:

$$\Delta x = \frac{6x_0}{\pi^2} exp\left(-\frac{\pi^2 Dt}{b^2}\right) = \frac{6x_0}{\pi^2} exp(-kt), \tag{18}$$

where

$$k = \frac{\pi^2 D}{b^2} \tag{19}$$

Consequently, from Eq. (19), it is possible to experimentally determine the oxygen diffusion coefficient D in the sample from the slope of the curve plotted in the coordinates $ln\ \Delta x = f(t)$.

3 Experimental

3.1 Synthesis of the YBCO Samples

For the experiments, the powder and pressed tablets of $YBa_2Cu_3O_{6+x}$ and $YBa_2Cu_3Fe_yO_{6+x}$ were synthesized following the same procedure described in reference [27]. In brief, the synthesis of the samples was conducted using the cryochemical method. Titrated solutions of $Ba(NO_2)_2$, $Y(NO_3)_3$, and $Cu(NO_3)_2$ were stoichiometrically combined. The solution was sprayed into liquid nitrogen using a pneumatic nozzle, and the resulting cryogranules were transferred to a metal tray. After evaporation of liquid nitrogen, sublimation drying was carried out in a sublimator SMN-15 (Usifroid, France) for 24 h (P_{O_2} = 0.1 mm Hg = 133. Pa). This freeze-drying process yielded salt powders with homogeneous distribution. The samples followed drying for thermal decomposition in a muffle furnace at 850 °C for 30 min.

The resulting calcined oxide powders, black in color, were ground in a milling mortar ("Pulviresette 02.102" from Fritsch, Germany). The average particle sizes of the powder were measured by means of dynamic light scattering analysis (Anallezette 22, Germany) and scanning electron microscopy (REM 100, USSR). According to them, the average size of the powder was 6.5 µm as it has been previously reported in reference [27].

The powders were pressed into tablets (P_{O_2}=1 GPa) and fired at 950 °C in air for 24 h. The cooling process was performed in a flow of oxygen, following a linear change in temperature from 950 to 350 °C for 2 days. For a complete oxidation, once the temperature reached 350 °C, it was maintained at this temperature under oxygen flow for another 24 h before being cooled in the oven.

3.2 Experimental Set-up

A homemade setup was meticulously assembled. It comprised a vacuum system of 10^{-5} Pa, a gas purification and injection system (for preparing gas mixtures with predetermined compositions), and an analytical component that records temporal changes in the gas pressure within the system during vacuum degassing. A schematic representation of the set-up is given in Fig. 1. To measure the pressure, an oxygen Pirani gauge was employed. The calibration of the Pirani gauge was performed by linking the oxygen pressure and the potentiometer signal. It was meticulously executed by systematically evacuating a portion of the gas introduced into the calibration volume (V_0 = 1200 cm^3). The exact determination of the volumes of various sections of the analytical part of the installation (V_x) was carried out using the pressure equalization method. This method involved measuring the initial gas pressure (P_1) and the resulting gas pressure (P_2) after connecting the analytical part with a calibrated volume (V_0) previously evacuated to a high vacuum under isothermal conditions, i.e.,

$$V_x = \frac{(P_1 - P_2)V_0}{P_2}$$

To conduct the experiments, the pre-weighed samples were placed in the reaction cell (see Fig. 1a). Subsequently, the air was evacuated to high vacuum (10^{-6} mmHg = 133.3 µPa) while simultaneously heating the cell. Purified and dried oxygen, passed through a silica gel column (SG), was then injected into the reactor space. Once the required temperature was reached,

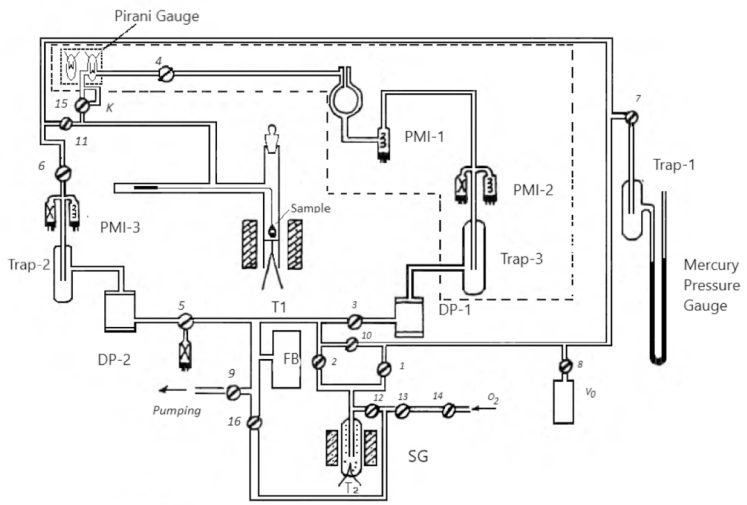

(a) (b)

Fig. 1 **a** Schematic representation of the set-up used for vacuum degassing measurement of the YBCO samples: *DP-1*, *DP-2*, diffusion pumps; 1–16, traps; trap-1,2,3, nitrogen traps; FB, fore-vacuum cylinder; T1, T2, thermocouples; SG, system for cleaning and drying supplied oxygen; PMI-1–3, ionization pressure sensors. The analytical part of the installation is highlighted with a dotted line. **b** Electrical circuit of the Pirani pressure gauge: *K* compensator; $R_{pgl} = 3.3$ Ohm; $R_{\kappa} = 3.3$ Ohm—resistance of the compensator thread; $R_1 = 10$ Ohm, $R_2 = 5$ kOhm, $R_3 = 33$ Ohm—resistance of the potentiometers and rheostat; $E = 12$ V direct current source

the sample (positioned in a quartz basket suspended on a thin nichrome thread using a vitrified magnetic core) was placed into the furnace zone and saturated with oxygen at a specified temperature and pressure for a predetermined time.

To monitor the level of saturation oxygen, the sample was expeditiously transferred from the furnace zone to the upper section of the cell, which is cooled by the evaporation of water coming from wet asbestos. After setting a specific degassing temperature, the sample was repositioned in the hot zone of the cell and subjected to degassing while undergoing continuous pumping. Throughout this process, variations in the partial pressure of oxygen in the system were monitored using the Pirani pressure gauge and the measurements automatically recorded.

The electrical circuit of the Pirani pressure gauge, depicted in Fig. 1b, represents a conventional Winston bridge circuit. To enhance the sensitivity of the pressure gauge, one of the bridge's arms was replaced with an exact duplicated pressure gauge featuring as compensator (denoted as K in the figure). The compensator was hermetically sealed following meticulous pumping to a pressure not exceeding 10^{-5} mmHg (1.3 mPa). Both, the compensator K and the pressure gauge lamp were immersed in a constant-temperature bath to mitigate the impact of ambient temperature fluctuations on the pressure gauge readings. The bridge circuit was configured using the resistances R_1 and R_2 shown in the figure. The pressure gauge lamp and the compensator K were meticulously fabricated from chemically inert materials (glass, with a sensitive element composed of thin platinum tape) and did not incorporate components operating at elevated temperatures. Consequently, during their operation, any surface processes capable of inducing alterations in the gas atmosphere composition were precluded.

3.3 Measurement on Vacuum Degassing

Experiments on vacuum degassing were conducted on the pressed samples of various densities $\rho = 4.5$ g/cm^3 (A) and $\rho = 5.5$ g/cm^3 (series B and C). The preliminary heat treatment of the tablets was as follows:

- Series A. Annealing for 2 h in oxygen ($P_{O_2} = 105$ mm Hg = 14 kPa) at 850 °C, which provides the initial value of the oxygen index $x_0 = 0.21$
- Series B. Annealing for 2 h in oxygen ($P_{O_2} = 153$ mm Hg = 20.4 kPa at 850 °C), which provides the initial value $x_0 = 0.24$
- Series C. Annealing for 1 h at 700 °C in an oxygen atmosphere ($P_{O_2} = 403$ mm Hg = 53.7 kPa), then slow cooling to 400 °C and subsequent annealing for 3 h at this temperature. In this case, $x_0 = 0.96$

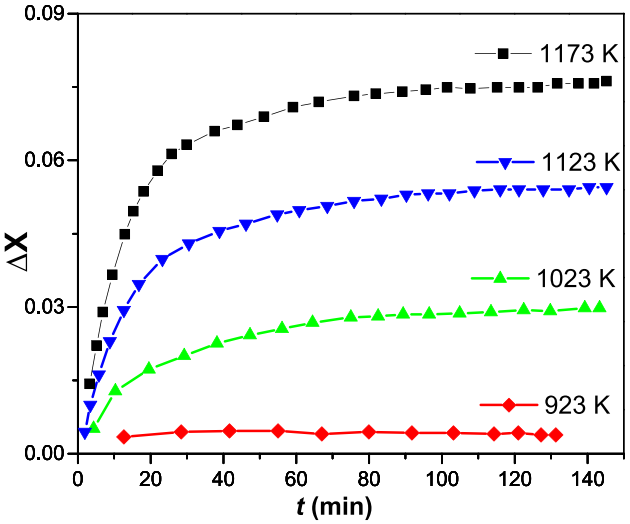

Fig. 2 Dependence of the amount of desorbed oxygen Δx with time during vacuum degassing of pressed $YBa_2Cu_3O_{6+x}$ tablets (series A)

The oxygen index value was determined from the Yamaguchi phase diagram [28].

The powdered samples (series D) underwent preliminary heat treatment at 850 °C (1123 K) and oxygen pressure P_{O_2} = 14 kPa. According to the phase diagram by Yamaguchi [28], that heat treatment corresponds to the oxygen index $x_0 = 0.21$. The degassing of the powder was carried out in the temperature range 450–800 °C (723–1073 K).

For series E, the heat treatment was conducted on the same samples with an initial value $x_0 = 0.31$, as follows. Firstly, heat the reactor to 800 °C and introduce oxygen ($P_{O_2} = 200$ kPa). Then, hold the sample at this temperature for 30 min and followed with slow cooling of the sample together with the furnace to 600 °C at a rate of 1.7°/min. Eventually, expose at 600 °C for 1 h.

4 Results and Discussions

4.1 Diffusion of Oxygen in $YBa_2Cu_3O_{6+x}$

The degassing kinetic curves of the sintered $YBa_2Cu_3O_{6+x}$ samples (series A) obtained from Eq. (13) are presented in Fig. 2. The obtained values of oxygen diffusion coefficients for series B and C are given in Table 1.

The values for the activation energy E_a and the pre-exponential factor D_0 were obtained with the help of Table 1, as follows:

- Series A: $E_a = (150 \pm 32)$ kJ/mol; $\ln D_0 = (0.73 \pm 0.06)$ cm^2/s
- Series B: $E_a = (149 \pm 42)$ kJ/mol; $\ln D_0 = (0.13 \pm 0.02)$ cm^2/s
- Series C: $E_a = (128 \pm 32)$ kJ/mol; $\ln D_0 = (0.57 \pm 0.06)$ cm^2/s

Figure 3 displays the kinetic curves of the released gas obtained under isothermal degassing conditions for the $YBa_2Cu_3O_{6+x}$ powder samples, series D and E. Table 2 presents their corresponding oxygen kinetic parameters.

Based on the $\Delta x(t)$ curves shown in Fig. 3, the gas evolution rate constants (k) and oxygen diffusion coefficients were determined. During the calculation of the diffusion coefficients, an average radius of the powder particles (b in Eq. (19)) as 6.5 μm is assumed. The $YBa_2Cu_3O_{6+x}$ powder used in the present work has been previously measured by means of dynamic light scattering analysis (Anallezette 22, Germany) and scanning electron microscopy (REM 100, USSR), as reported in reference [27]. Thus, the obtained values are listed in Table 2.

Note that by comparing the data presented in Tables 1 and 2, the values of the diffusion coefficients in the powder are two to three orders of magnitude smaller than in the tablet samples:

Table 1 Oxygen diffusion coefficients obtained for pressed samples $YBa_2Cu_3O_{6+x}$

	D (cm^2/s)		
T(K)	$\rho = 4.55$ (g/cm^3)	$\rho = 5.55$ (g/cm^3)	
	Series A ($x = 0.21$)	Series B ($x = 0.24$)	Series C ($x = 0.96$)
923	$(5.16 \pm 0.13) \times 10^{-8}$ $(3.43 \pm 0.21) \times 10^{-8}$	-	$(1.13 \pm 0.02) \times 10^{-8}$
973		-	$(5.96 \pm 0.85) \times 10^{-8}$
1023	$(8.7 \pm 1.5) \times 10^{-8}$ $(2.43 \pm 1.5) \times 10^{-8}$	$(2.78 \pm 0.09) \times 10^{-8}$	$(7.02 \pm 1.04) \times 10^{-8}$
1073		$(9.31 \pm 0.67) \times 10^{-8}$	$(1.37 \pm 0.3) \times 10^{-7}$
1123	$(4.43 \pm 0.07) \times 10^{-7}$	$(1.34 \pm 0.1) \times 10^{-7}$	-
1173	$(8.64 \pm 0.21) \times 10^{-7}$	-	-

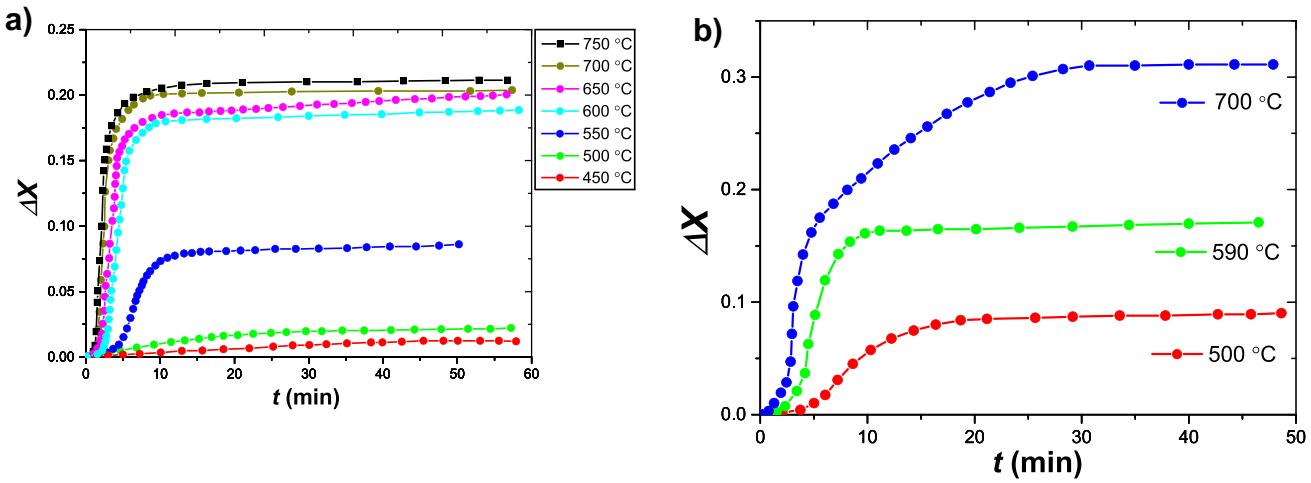

Fig. 3 $\Delta x(t)$ curves for the $YBa_2Cu_3O_{6+x}$ samples: **a** series D and **b** series E

– Series D: $E_a = (59.21 \pm 5.11)$ kJ/mol; $\ln D_0 = (-5.75 \pm 0.30)$ cm^2/s
– Series E: $E_a = (19.70 \pm 4.70)$ kJ/mol; $\ln D_0 = (-7.88 \pm 0.29)$ cm^2/s

By comparing the degassing isotherms obtained for the pressed samples, series A, B, and C, it is revealed that the quantity of oxygen desorbed during vacuum degassing is contingent upon the density of the pressed tablets. High tablet density results in low amount of desorbed oxygen. For instance, in series A ($\rho = 4.5$ g/cm^3), the quantity of released oxygen ranges from 2% at 923 K to 35% at 1177 K of the initial value x_0. Conversely, for the high-density (extruded) samples, series B and C ($\rho = 5.5$ g/cm^3), the desorbed oxygen amount is lower, varying from 6% at 923 K to 19% at 1177 K.

Table 2 Oxygen diffusion coefficients obtained for $YBa_2Cu_3O_{6+x}$ powders samples (series D and E)

T (K)	k (s^{-1})	D (cm^2/s)
Series D		
723	$(1.17 \pm 0.06) \times 10^{-3}$	$(5.00 \pm 0.26) \times 10^{-11}$
773	$(5.98 \pm 1.12) \times 10^{-3}$	$(2.57 \pm 0.48) \times 10^{-10}$
773	$(4.75 \pm 1.4) \times 10^{-3}$	$(2.03 \pm 0.6) \times 10^{-10}$
823	$(7.77 \pm 4.6) \times 10^{-3}$	$(3.33 \pm 1.97) \times 10^{-10}$
873	$(1.21 \pm 0.96) \times 10^{-2}$	$(5.2 \pm 4.11) \times 10^{-10}$
893	$(1.98 \pm 0.44) \times 10^{-2}$	$(8.49 \pm 1.88) \times 10^{-10}$
923	$(2.18 \pm 2.26) \times 10^{-2}$	$(9.37 \pm 9.71) \times 10^{-10}$
973	$(2.38 \pm 1.50) \times 10^{-2}$	$(1.02 \pm 0.64) \times 10^{-9}$
973	$(2.71 \pm 0.35) \times 10^{-2}$	$(1.16 \pm 0.15) \times 10^{-9}$
973	$(2.85 \pm 0.71) \times 10^{-2}$	$(1.22 \pm 0.30) \times 10^{-9}$
1023	$(4.00 \pm 2.02) \times 10^{-2}$	$(1.72 \pm 0.87) \times 10^{-9}$
1023	$(3.82 \pm 1.99) \times 10^{-2}$	$(1.64 \pm 0.85) \times 10^{-9}$
Series E		
773	$(1.48 \pm 0.09) \times 10^{-2}$	$(6.37 \pm 0.37) \times 10^{-10}$
863	$(1.90 \pm 0.12) \times 10^{-2}$	$(8.16 \pm 0.50) \times 10^{-10}$
973	$(2.79 \pm 0.18) \times 10^{-2}$	$(1.20 \pm 0.08) \times 10^{-10}$

For the powdered samples, series D and E (see Fig. 3), the aforementioned trend of increasing the amount of desorbed oxygen from the sample (Δx) with rising degassing temperature persists.

In addition, within the temperature range 550–600 °C, over 50% of the oxygen is released during the first 60 min. Below 550 °C, the quantity of released oxygen does not surpass 40% of the initial value x_0. At elevated vacuum degassing temperatures, nearly 100% of the absorbed oxygen is liberated. This suggests that the absorption and desorption of the oxygen in $YBa_2Cu_3O_{6+x}$ powders occur at a significantly faster rate compared to the pressed $YBa_2Cu_3O_{6+x}$ tablets.

On the other hand, the analysis indicates that for the pressed samples, series A, B, and C, not all weakly bound oxygen is desorbed during isothermal vacuum degassing, i.e., $\Delta x \ll x_0$. In this situation, the graphs of the $\Delta x(t)$ dependences (Fig. 2) reveal two distinct stages of degassing kinetics. It is evident that the primary portion of the desorbed oxygen (approximately 90% of Δx) is liberated during the initial stage, corresponding to roughly the first 25 min from the moment the sample is placed in the reactor and the degassing of series A, B, and C starts. Conversely, the majority of absorbed oxygen in the powdered samples (series D and E) is desorbed within the first 10 min (see Fig. 3). The residual portion of absorbed oxygen undergoes degassing in the second stage, characterized by slower degassing kinetics.

It is evident that the kinetics of degassing oxygen at these stages differs. The initial degassing stage can be elucidated by considering a homogeneous diffusion from a semi-confined sample with zero concentration at the surface. In

this case, the diffusion coefficients for the oxygen can be determined by Eq. (13). The pronounced deceleration in the kinetics of releasing gas during the second stage, occurring after a certain period of time ($t \approx 25$ min) from the initiation of the degassing, may be attributed to the formation and growth of a new "phase" on the surface of the sample, likely attributed to reactive diffusion with a lower diffusion coefficient than that observed in the first stage.

It is noteworthy that the presence of a "surface barrier" impeding free gas exchange in YBCO has been extensively discussed for decades [29–32]. This barrier may be associated either with a specific surface structure or with some energy parameters. For instance, by using electron microscopy, some researchers have demonstrated the formation of a ceramic layer depleted in oxygen on the surface of the $YBa_2Cu_3O_{6+x}$, exhibiting new physical properties such as high electrical resistance [33]. It was further revealed that the growth of this layer (new phase) occurs parallel to the *c*-axis indicating that its formation kinetics is largely influenced by the transport properties of oxygen along the *c*-axis [33]. Additionally, it has been established that the diffusion coefficient along the *a*- and *b*-axes is three to four orders of magnitude greater than along the *c*-axis [34]. Figure 4 shows the comparison of the activation energy (E_a) values and the obtained pre-exponential factor D_o in the present work with those reported in the literature [34].

4.2 Diffusion of Oxygen in $YBa_2Cu_{3-y}Fe_yO_{6+x}$.

In the investigation of high-temperature superconducting compounds, the influence of doping with various chemical elements on their physical properties holds significant interest [35, 36]. In the present work, particular attention is given to the impact of the substitution of Cu by Fe atoms on the oxygen kinetic parameters in $YBa_2Cu_3O_{6+x}$. The Cu atoms in the YBCO structure occupy two distinct regions: forming CuO_2 planes alongside the *ab* plane and forming CuO chains in the *c*-direction. Substituting Cu with other transition metals may offer insights into the nature of the superconductivity of this system. To validate this notion, the diffusion properties of oxygen in $YBa_2Cu_{3-y}Fe_yO_{6+x}$ (with $y = 0.03$, 0.06, 0.15, and 0.30) obtained using standard ceramic technology are investigated here. The oxygen diffusion parameters are determined under conditions of isothermal gas evolution in vacuum using the Manometric method described above in the temperature range 450–700 °C, and based on Eq. (13). All samples were pre-saturated with oxygen at 850 °C and under 14 kPa pressure for 0.5 h, corresponding to the initial oxygen non-stoichiometry $X_0 = 0.21$.

Figure 5 illustrates the activation energy dependence on the iron concentration in the structure of YBCO. Table 3 presents the oxygen diffusion parameters for the pressed $YBa_2Cu_{3-y}Fe_yO_{6+x}$ pellets (with $y = 0.03$, 0.06, 0.15, and 0.30) estimated from their corresponding experimental dynamic degassing isotherms.

According to the data presented in Fig. 5, it is evident that the increase in iron concentration significantly impedes oxygen exchange in $YBa_2Cu_{3-y}Fe_yO_{6+x}$, as indicated by the decrease in the amount of released oxygen with increasing *y*. It has been established that when copper is substituted by Fe in $YBa_2Cu_3O_7$, iron atoms predominantly occupy the Cu(1) positions [19]. This substitution leads to a modification in the oxygen stoichiometry of the samples due to the emergence of new oxygen states between Cu(1) atoms along the crystallographic *a*-axis [37]. The discrepancy in the properties of Fe and Cu ions and their oxygen environments is manifested in the energy states of oxygen in iron-doped HTSC compounds. This is further supported by

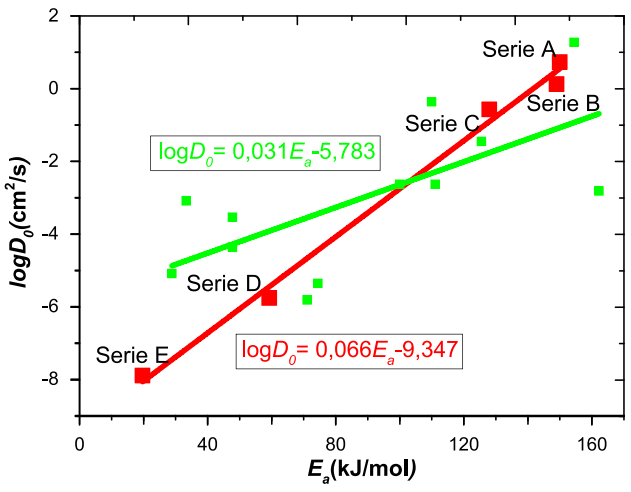

Fig. 4 Comparison of the obtained E_a and D_0 values for samples A, B, and C with the data reported in the literature. The red dots are the data obtained in the present work, whereas the green dots are taken from reference [33]

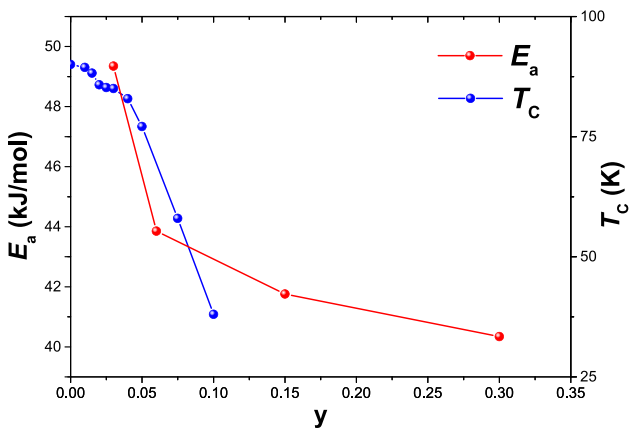

Fig. 5 Dependence of critical temperature of superconducting transition T_c [36] and activation energy E_a on iron concentration *y* in $YBa_2Cu_{3-y}Fe_yO_{6+x}$

Table 3 Values of activation energy (E_a) and pre-exponential multiplier D_0 for oxygen diffusion obtained for pressed $YBa_2Cu_{3-y}Fe_yO_{6+x}$ samples (with $y = 0.03$, 0.06, 0.15, and 0.30)

y	E_a (kJ/mol)	Log(D_0) (cm^2/s)
0.03	49.35 ± 7.52	−6.44 ± 0.44
0.06	43.85 ± 15.17	−6.78 ± 0.92
0.15	41.76 ± 7.56	−6.87 ± 0.46
0.3	40.34 ± 2.95	−6.89 ± 0.19

thermogravimetry data [38], indicating that the substitution of Cu by Fe impedes the release of oxygen from the samples.

A comparison of the obtained data on the dependence of activation energy with the data on the dependence of the critical temperature on the iron content according to reference [37] is also presented in the figure. Overall, both the activation energy E_a and T_c exhibit a similar tendency to decrease with increasing iron content in $YBa_2Cu_{3-y}Fe_yO_{6+x}$.

5 Conclusions

The kinetic parameters of oxygen in the $YBa_2Cu_3O_{6+x}$ system can be confidently described by the Manometric method. This approach is also effective for investigating the kinetic parameters of Fe-doped YBCO. An experimental discrepancy was observed in the diffusion coefficients calculated from the isothermal curves of vacuum degassing for pressed samples (70% of theoretical for series A and 85% of theoretical for series B and C) compared to powder $YBa_2Cu_3O_{6+x}$. This difference might be originated by the presence of "easy paths" such as grain boundaries, microcracks, and micropores in the pressed samples, facilitating rapid oxygen diffusion during the initial stage. During degassing process, the relative yield of oxygen in the powder also demonstrates a monotonic increase with rising temperature. However, unlike tablets, at 973 K and above, 100% of the absorbed oxygen is released from the sample. The experiments have further revealed that an increase in the initial value of nonstoichiometric oxygen (x_0) in $YBa_2Cu_3O_{6+x}$ powders influences the value of the activation energy (E_a), underestimating it by nearly three times, along with a corresponding alteration in the pre-exponential factor (D_0). However, the values of the diffusion coefficients remain almost unchanged in absolute terms. As for the $YBa_2Cu_{3-y}Fe_yO_{6+x}$ samples under isothermal conditions of vacuum degassing, it was found that the rate of releasing oxygen can be described by an exponential law, and the amount of desorbed oxygen monotonically increases with increasing degassing temperature. Eventually, the replacement of Cu with Fe in the YBCO structure significantly affects the oxygen exchange, as evidenced by a decrease in the amount of released oxygen with y in this compound.

Supplementary Information The online version contains supplementary material available at https://doi.org/10.1007/s10948-024-06796-5.

Acknowledgements J. Kargin thanks professors Andreev L.A., Nechaev Yu.S. and Minaev Yu.A. from the Moscow Institute of Steel and Alloys (MISIS) for helpful discussions.

Author Contributions Data acquisition, methodology, data curation and formal analysis (J. Kargin, H.E Sanchez Cornejo, K. Zhangozin, T. Zhanabergenov and Zh. Kassymkhanov), conceptualization, interpretation, validation, data curation and visualization (Jiwon Seo, S.N. Holmes, C.H.W. Barnes, J. Albino Aguiar and L. De Los Santos Valladares) and all authors have contributed in writing the manuscript.

Funding The work in Peru has been supported by the Peruvian Agency CONCYTEC, grant No. PE501079382-2022-PROCIENCIA. The work in Brazil has been supported by the PROFESSOR VISITANTE Programme N°. 13/2022 of the Universidade Federal de Pernambuco, Brazil, Contract No. 062 /2022 (Process no. 23076.101469/2021–69). J. Kargin received support from the JSC "Center for International Programs" of the Republic of Kazakhstan under the International Programme "500 scientists," Agreement for Scientific Internship No. 7971 dated July 18, 2023.

Data Availability No datasets were generated or analysed during the current study.

Declarations

Competing Interests The authors declare no competing interests.

References

1. Netchaev, Y.S., Zhangozin, K.N., Minaev, Y.A., Andreev, L.A., Kargin, D.B., Konovalov, N.G., Lykhin, V.A.: On the nature of the phase transitions at elevated temperature in the 123 type ceramics. Physica C: Supercond. Appl. **185–189**, 1735–1736 (1991). https://doi.org/10.1016/0921-4534(91)90994-A
2. De Los Santos Valladares, L., Bustamante Domínguez, A., Flores Santibañez, J., González González, J.C.: Preparation and characterization of the superconductor $CaLaBaCu_{2.8}(PO_4)_{0.2}O_{6.2}$ compound. Physica C: Supercond. Appl. **408–410**, 44–45 (2004). https://doi.org/10.1016/j.physc.2004.02.032
3. Bustamante Domínguez, A., Bellido Quispe, R., De Los Santos Valladares, L., González, J.C.: Preparation and characterization of the superconductor $CaLaBaCu_{2.8}(BO_3)_{0.2}O_{6.4}$ compound. Physica C: Supercond. Appl. **408–410**, 884–885 (2004). https://doi.org/10.1016/j.physc.2004.03.231

4. Barinotto, V.H., Willems, B.L., Bustamante Domínguez, A.G., De Los Santos Valladares, L., González González, J.C.: Preparation and characterization of the superconductor $[Y_{0.8}Ca_{0.2}]SrBaCu_{2.8}(BO_3)_{0.2}O_{6.4}$ compound. Physica C: Supercond. Appl. **408–410**, 58–59 (2004). https://doi.org/10.1016/j.physc.2004.02.052
5. Bustamante Domínguez, A., Osorio Anaya, A.M., De Los Santos Valladares, L., Carhuancho, H., González, J.C., Cernicchiario, G. , Feijoo Levano, J.A.: Synthesis of $YBa_2Cu_3O_{7-\delta}$ using oxalate precursor and sol-gel method. Adv. Sci. Technol. **47**, 37–42 (2006). https://www.academia.edu/11620456/Synthesis_of_YBa2Cu3O7_%CE%B4_Using_Oxalate_Precursors_and_Sol_Gel_Method
6. Sanchez Cornejo, H., De Los Santos Valladares, L., Barnes, C.H.W., et al.: Texture and magnetic anisotropy of $YBa_2Cu_3O_{7-x}$ film on MgO substrate. J. Mater. Sci: Mater. Electron. **31**, 21108–21117 (2020). https://doi.org/10.1007/s10854-020-04623-w
7. Bustamante Domínguez, A., Osorio Anaya, A.M., De Los Santos Valladares, L., Garcia Dulanto, J., González, J.C., Barnes, C.H.W., Azuma, Y., Majima, Y., Albino Aguiar, J.: Epitaxial growth of $YBa_2Cu_3O_7$ on $SrTiO_3$ (100) by direct solution precursor deposition. J. Phys.: Conf. Ser. **507**, 012005 (2014). https://doi.org/10.1088/1742-6596/507/1/012005
8. De Los Santos Valladares, L., González, J.C., Bustamante Domínguez, A., Osorio Anaya, A.M., Sanchez Cornejo, H., Holmes, S., Albino Aguiar, J., Barnes, C.H.W.: A fluorine-free oxalate route for the chemical solution deposition of $YBa_2Cu_3O_7$ films in Superconductors, edited by Alexander Gabovich, ISBN 978–953–51–4163–1. Intech, Chapter **3**, 35–53, (2015). https://doi.org/10.5772/59359
9. Sanchez Cornejo, H., De Los Santos Valladares, L., Kamboj, V.S., Bustamante Dominguez, A., González, J.C., Osorio Anaya, A.M., Moreno, N.O., Beere, H.E., Ritchie, D.A., Newton, P.J., Barnes, C.H.W.: Texture and terahertz analysis of $YBa_2Cu_3O_7$ grown onto $LaAlO_3$ by the chemical solution deposition technique. Heat Treat. Surf. Eng. **3**(1), 1–8 (2021). https://doi.org/10.1080/25787616.2021.2022294
10. Nechaev, Y.S., Lykhin, V.A., Zhangozin, K.N., Kargin, D.B., Khramova, N.V.: Thermodynamic and kinetic characteristics of oxygen in $YBa_2Cu_3O_{6+x}$ superconducting ceramics. Zhurnal Fizicheskoi Khimii. **68**(9), 1690–1696 (1994). ISSN 0044–4537 (in Russian)
11. Bustamante Dominguez, A.G., Sanchez Cornejo, H.E., González, J.C., Ingo, G.M., Riccucci, C., Di Carlo, G., Pascucci, M., Albino Aguiar, J., Barnes, C.H.W., De Los Santos Valladares, L.: Aging and environmental effects on the superconductor $[Y_{1-x}Ca_x]SrBaCu_{2.80}(BO_3)_{0.20}O_y$ with $0.10 \leq x \leq 0.50$. J. Supercond. Novel Magn. (2024). https://doi.org/10.1007/s10948-024-06745-2
12. Domínguez, A.B., De Los Santos Valladares, L., Cornejo, H.S., et al.: $YBa_2Cu_3O_7$ films grown onto $SrTiO_3$ and YSZ substrates by chemical solution deposition of trifluoroacetates. J. Electroceram. **47**, 15–22 (2021). https://doi.org/10.1007/s10832-021-00256-5
13. Tretyakov, Y.D., Gudilin, E.A.: Chemical principles of the metall-oxide superconductors preparation. Uspekhi Khimii. **69**(1), 3–40 (2000), ISSN 00421308 (in Russian)
14. Petrykin, V.V, Oleynikov, N.N.,. Ketsko, V.A.: Oxidation of yttrium barium cuprate $YBa_2Cu_3O_{6.09}$ under polythermal conditions. Inorg. Mater. **32**(2),168–173 (1996). ISSN 00201685 (in Russian)
15. Tong, B.T., Lo, W.: Oxygen diffusion in Yba2Cu3Ox: An isithermal thermogravimetric study. Physica C: Supercond. Appl. **174**(4–6), 463–466 (1991). https://doi.org/10.1016/0921-4534(91)91584-Q
16. Mozhaev, A.P., Mazo, G., Galkin, A., Khramova, N.V.: Phase stability and oxygen diffusion in $RBa_2Cu_3O_{6+x}$ (R = Y, Nd). Russ. J. Inorg. Chem. **41**(6), 881–885 (1996). ISSN 00360236 (in Russian)
17. Bredikhin, S.I., Emel'chenko, G.A., Shekhtman, V.Sh., Zhokhov, A.A., Carter, S., Chater, R.J., Kilher, J.A. Steele, B.C.H.: Anisotropy of oxygen self-diffusion in $YBa_2Cu_3O_{7-\delta}$ single crystals. Physica C: Supercond. Appl. **179**(4–6), 286–290 (1991). https://doi.org/10.1016/0921-4534(91)92173-9
18. Xie X.M., Chen T.G., Wu Z.L.: Oxygen diffusion in the superconducting oxide $YBa_2Cu_3O_{7-x}$. Phys. Rev. B.: Condens. Matter. **40**, 4559–4556 (1989). https://doi.org/10.1103/PhysRevB.40.4549
19. Rothman S.J., Routbort J.L., Welp U., Baker J.E.: Anisotropy of oxygen tracer diffusion in single-crystal $YBa_2Cu_3O_{7-\delta}$. Phys. Rev. B.: Condens. Matter. **44**, 2326–2333 (1991). https://doi.org/10.1103/PhysRevB.44.2326
20. Erb, A., Greb, B., Muller-Vogt, G.: In-situ resistivity measurements during the oxygenation of $YBa_2Cu_3O_{7-\delta}$ and $Gd_{0.8}Y_{0.2}Ba_2Cu_3O_{7-\delta}$ single crystals. Physica C: Supercond. Appl. **259**(1–2), 83–91 (1996). https://doi.org/10.1016/0921-4534(96)00008-1
21. Shi; D., Krucpzak, J., Tang, M., Chen; N., Bhadra, R.: Oxygen diffusion and phase transformation in $YBa_2Cu_3O_{7-x}$. J. Appl. Phys. **66**(9), 4325–4328 (1989). https://doi.org/10.1063/1.343979
22. Yamada, Y., Shiohara, Y.: Continuous crystal growth of $YBa_2Cu_3O_{7-x}$ by the modified top-seeded crystal pulling method. Physica C: Supercond. Appl. **217**(1–2), 182–188 (1993). https://doi.org/10.1016/0921-4534(93)90810-D
23. Kemnitz, E., Galkin, A.A., Olesch, T., Sheurel,l S., Mozhaev, A.P., Mazo, G.N.: Oxygen diffusion and isotope exchange behaviour of $NdBa_2Cu_3O_{7-x}$. J. Thermal. Anal. **48**, 997–1010 (1997). https://doi.org/10.1007/BF01979149
24. Galkin, A., Mazo, G., Lunin, V., Sheurel, S., Kemnitc, E.: Mobility of oxygen in multicomponent oxide systems $RBa_2Cu_3O_y$ (R = Nd, Ho, and Y). Zhournal Fizicheskoi khimii. **72**(9),1618–1624 (1998). ISSN 00444537 (in Russian)
25. Fontain, D., Ceder, G., Asta, M.: Thermodynamics of oxygen ordering in $YBa_2Cu_3O_z$. J. Less Common Metals. **164–165**(1), 108–123 (1990). https://doi.org/10.1016/0022-5088(90)90204-W
26. Bokshtein, B.S.: Diffusion in metals. Moscow, Metallurgia (1978) (in Russian)
27. Mozhaev, A.P., Chernyaev, S.V.: Oxygen diffusion in $YBa_2Cu_3O_{6+x}$ ceramics. J. Mater. Chem. **4**, 1107–1110 (1994). https://doi.org/10.1039/JM9940401107
28. Yamaguchi, S., Terabe, K, Saito, A.: Determination on nonstoichiometry in $YBa_2Cu_3O_{7-X}$. Jap. J Appl. Phys. **27**(2), 179–181 (1988). https://doi.org/10.1143/JJAP.27.L179
29. Elkin, BSh., Baikov, Yu.M.: Kinetics of isotope exchange of dioxygen with a powdered high-temperature superconducting material $Ba_2YCu_3O_{7-x}$. React. Kinet. Catal. Lett. **40**, 19–24 (1989). https://doi.org/10.1007/BF02235132
30. Netchaev, Y.S., Zhangozin, K.N., Minaev, Y.A., Andreev, L.A., Kargin, D.B.: On the phase diagram of the supercondacting ceramics 123 type. J. Physique III, France. **1**(10), 1663–1668 (1991). ⟨https://doi.org/10.1051/jp3:1991219⟩. ⟨jpa-00248689⟩
31. Andreev, L.A., Nechaev, Y.S., Minaev, Y.A., Sigitov, EV., Zhangozin, K.N.; Kargin, D.B., Lykhin, V.A., Konovalov, N.T.: Kinetics of oxygen isolation under vacuum degasification of $YBa_2Cu_3O_y$ ceramics. Zhurnal Fizicheskoi Khimii. **66**(12), 3238–3243 (1992). Accession Number WoS:A1992KH82500014, ISSN 0044–4537 (in Russian)
32. De Los Santos Valladares, L, Bustamante Dominguez, A.G, Llandro, J, Suzuki, S., Mitrelias, T., Bellido Quispe, R., Barnes, C.H.W., Majima, Y., Attaching thiolated superconductor grains on gold surfaces for nanoelectronics applications. Jpn. J. Appl. Phys. **49**, 093102 (2010). https://doi.org/10.1143/JJAP.49.093102
33. Geym, A.K., Dubonos, S.V., Panin, G.N., Klimenko, G.L.: Electron microscopic studies of the properties of a dielectric on the surface of a high-temperature superconductor. Phys. Met. Metallogr. **69**(3), 81–87 (1990). ISSN 0031918X (in Russian)

34. Chernyaev, S., Rudnitsky, L., Mozhaev, A.P. : Oxygen non-stoichiometry and diffusion in $RBa_2Cu_3O_{6+X}$ (R=Y, Gd, Ho) investigated by TG method. J. Therm. Anal. **48**, 941–950 (1997). https://doi.org/10.1007/BF01979144
35. Yamada, Y., Oda, Y., Kawaji, N., Kunisuke, A., Hideki, Y.: Magnetic properties of O_2-annealed $YBa_2(Cu_{1-x}M_x)_3O_y$ with M=Fe, Co and Ni. J. Phys. Soc. Japan. **58**, 3053–3056 (1989). https://doi.org/10.1143/JPSJ.58.3053
36. Del Moral, A., Ibarra, M.R., Algarabel, P.A., Arnaudas, J.I.: Magnetostriction and thermal expansion of high-Tc magnetic superconductors $REBa_2Cu_3O_{7-x}$ (RE = Sm, Eu, Gd, Dy, Ho, Er, Tm and Y). Physica C: Supercond. Appl. **161**(1), 48–58 (1989). https://doi.org/10.1016/0921-4534(89)90040-3
37. Tarascon, J.M., Barboux, P., Miceli, P.F., Greene, L.H., Hull, G.W., Eibschutz, M., Sunshine, S.A.: Structural and physical properties of the metal (M) substituted $YBa_2Cu_{3-x}M_xO_{7-y}$ perovskite. Phys. Rev. B **37**, 7458–7469 (1988). https://doi.org/10.1103/PhysRevB.37.7458
38. Xu, Y., Suenaga, M., Tafto, J., Sabatini, R.L, Moodenbaugh, A.R.: Microstructure, lattice parameters, and superconductivity of $YBa_2(Cu_{1-x}Fe_x)_3O_{7-\delta}$ for 0~x~0.33. Phys. Rev. B. **39**, 6667–6680 (1989). https://doi.org/10.1103/PhysRevB.39.6667